



Highly stable commercial-level mass-loaded supercapacitor using *Datura stramonium* seeds derived activated microporous biocarbon

A. Kumaravel¹ · S. Sathyamoorthi² · S. Sadhana³

Received: 19 July 2023 / Revised: 15 August 2023 / Accepted: 23 August 2023
© The Author(s), under exclusive licence to Springer-Verlag GmbH Germany, part of Springer Nature 2023

Abstract

The exploration of biocarbon using various bio-resources has received great importance as the awareness of environmentally benign energy storage technologies is increasing drastically. Additionally, the active mass loading of the electrode in the supercapacitors has recently gained great importance as it meets the industrial requirement as well as provides practical electrochemical performance. In this study, we synthesized activated biocarbon using *Datura stramonium* seeds through pyrolysis with chemical activation. To achieve real-world performance, biocarbon mass loadings at commercial levels ($\geq 10 \text{ mg cm}^{-2}$) were used in the fabrication of symmetrical supercapacitors. The single electrode-specific capacitance of 114 F g^{-1} was estimated at 1.2 V with excellent coulombic efficiency of 99% and energy efficiency of 82%. We obtained the maximum specific energy of 5.6 Wh kg^{-1} at 0.1 A g^{-1} and specific power of 980 W kg^{-1} . Excellent specific capacitance retention of 100% is noted at the end of 10,000 GCPL cycles at 1.0 A g^{-1} , indicating that symmetrical supercapacitors with synthesized biocarbon possess high stability.

Keywords Biocarbon · Activated carbon · Supercapacitor · Commercial-level mass load · *Datura stramonium* seeds

Introduction

Ever-increasing concerns about the environmental impact of unrestricted use of the resource to meet the demand for energy storage technologies necessitate eco-friendly materials for high-performance energy storage applications [1]. Converting solid waste into biochar or biocarbon by thermal treatment (300 to 900 °C) in the inert atmosphere has great advantages to the circular economy [1]. Appealing properties of biocarbon such as high surface area, porosity, functional groups, presence of hetero atoms and metallic elements, etc. encourage its applicability in numerous fields, including

energy storage. Especially biocarbon has been extensively employed as electrode material in electrical double-layer capacitors. High specific power, fast charge–discharge rate and long-term stability are advantages of these supercapacitors. Thus, they act as supplements for other energy storage devices in portable devices and hybrid vehicles. Characteristic porous networks of natural biomass resources become a favourite starting material for the synthesis of biocarbon with desired high surface area with porosity. Not limited to rice husk [2], corn stover [3], casein [4], aloe vera [5], rice straw [6], cinnamon sticks [7], corn cob [8], soybean pods [9], potato waste residue [10], wood waste [11], onion leaves [12], walnut shell [13], pistachio nutshell [14], lotus seedpods [15] and egg yolk [16], numerous biomasses are employed to synthesis of biocarbon.

So far synthesis of biocarbon based on the circular economy as accumulation and the effective disposal of these biowastes are major concerns, while *Datura stramonium* is a toxic invasive plant which is grown freely in any type of soil with high seed output [17, 18]. A lifetime of a plant is 40 years with up to 30,000 thousand seed production in its lifetime. Though *Datura stramonium* possesses some medicinal benefits, the toxic effect is the dominant concern in modern medicine. There are several incidents related to

✉ A. Kumaravel
kumaravelchem@gmail.com

✉ S. Sathyamoorthi
avanissm@gmail.com

¹ Functional Materials Laboratory, Department of Chemistry, PSG Institute of Technology and Applied Research, Neelambur, Coimbatore, Tamilnadu 641062, India

² Department of Chemistry, Ultra Arts and Science College, Madurai, Tamilnadu 625104, India

³ Department of Chemistry, PSGR Krishnammal College for Women, Coimbatore, Tamilnadu, India

toxic effects documented in history. Recently, *Datura stramonium* contaminated humanitarian relief food resulting in a large outbreak in Uganda during 2019 as a result of its severe poisoning effect [17]. Similarly, another incident was reported in Australia on December 2022 where nearly 200 people were poisoned as a result of consumption of *Datura stramonium*-contaminated spinach. Toxicity cannot be destroyed by boiling or drying out any parts of the plant [18]. But thermal weeding at 120 °C more than 180 s can destroy the plant and its toxicity [19]. An enormous amount of carbonaceous material can be produced as this plant grew up to 5 feet very quickly without any effort. Keeping all these concerns in mind, the synthesis of carbon material from the *Datura stramonium* plant was carried out which is beneficial in both economic and environmental fronts.

Recently, the active mass loading of the electrode in the supercapacitors ($\geq 10 \text{ mg cm}^{-2}$) has received great importance as it meets the industrial requirement and provides practical electrochemical performance [20]. However, the gap between the research and the commercial devices has been widely recognized. Supercapacitors with low mass loading of active material led to overestimation of electrochemical performance. In the present work, we employed *Datura stramonium* seeds for the synthesis of biocarbon. To achieve real-world performance, commercial levels ($\geq 10 \text{ mg cm}^{-2}$) mass loaded biocarbon electrodes were used in the fabrication of symmetrical supercapacitors. The synthesized biocarbon was characterized using laser Raman, Fourier Transform Infra-Red Spectroscopy (FTIR), X-Ray diffraction (XRD), Brunauer–Emmett–Teller (BET) and Scanning Electron Microscopy (SEM) techniques. 1.0 M $\text{Na}_2\text{SO}_{4(\text{aq})}$ was used as an electrolyte to fabricate supercapacitors. Electrochemical techniques such as electrochemical impedance spectroscopy (EIS), cyclic voltammetry (CV) and galvanostatic charge–discharge with potential limitation (GCPL) were used to evaluate the electrochemical performance of the symmetrical supercapacitors. The long-term stability of supercapacitors was evaluated by performing up to 10,000 GCPL cycles at 1.0 A g^{-1} .

Experimental section

Materials

The following analytical grade chemicals were purchased from Merck India Ltd., Calcium chloride (CaCl_2), hydrochloric acid (HCl), potassium hydroxide (KOH), sodium sulphate (Na_2SO_4), poly(vinylidene fluoride-co-hexafluoropropylene) (PVDF), N-methyl-2-pyrrolidone (NMP) and carbon black were used without any further purification. Double distilled (DD) water was prepared by using a double

distillation setup available in the laboratory, which was used for synthesizing biocarbon and preparing the electrolyte.

Synthesis of biocarbon

Synthesis of biocarbon was carried out as per the reported procedure with slight modification [21]. Collected *Datura stramonium* seeds with their shells were cleaned with DD water to remove any adhered soli material. Thoroughly washed seeds were dried in the sunlight for 2 days. The dry samples were grounded well, using mortar. The preparation of charcoal was carried out at 300 °C for 5 h in a muffle furnace. The activation of charcoal was carried out by mixing it with 25 wt% CaCl_2 solution over a period of 20 h. The obtained sample was washed thoroughly with DD water and dried overnight in an oven at 110 °C. Further, the carbon was activated chemically by impregnating carbon in a KOH solution. The procedure for chemical activation was carried out as follows: 5 g of activated carbon and 5 g of KOH were mixed with 15 ml of DD water at 60 °C. The wet slurry was dried at 110 °C for 14 h. Carbonization was achieved at 600 °C for 1 h in the muffle furnace in the nitrogen atmosphere. The carbonization temperature was attained with a temperature interval of 10 °C from room temperature. The sample was brought down to room temperature by gradual reduction of temperature under the nitrogen atmosphere. The pyrolyzed sample was neutralized and washed using a dilute HCl solution until the pH of the mixture reached neutral. The neutralized sample was washed with plenty of DD water repeatedly until it was free from chloride ions. Silver nitrate solution was used as a reagent to monitor the removal of the chloride ions. In the end, the sample was dried overnight and used to construct the supercapacitor.

Characterization of biocarbon

A field-emission scanning electron microscopy (FE-SEM, ZEISS Sigma) was employed to examine the surface morphological characterization of the synthesized biocarbon. Fourier transforms infrared spectrometer (FTIR—Shimadzu) was used for effective carbonization and reduction via the presence of surface functionalities of biocarbon. The laser Raman spectrum of biocarbon was recorded with the excitation wavelength of 400 nm using WiTec alpha 300, Raman spectrometer. Malvern Panalytical's X-ray diffraction diffractometer with Ni-filtered Cu-K radiation ($\lambda = 1.54056 \text{ \AA}$) was used to record the XRD pattern of the sample. Peak fitting was carried out using Origin Pro 8.5. Nitrogen gas sorption analysis (GSA) in liquid nitrogen at 77 K was used to quantify the surface area, pore volume and the distribution pattern of pores. JWGB ·Densi 100 model, instrument was used to conduct the GSA analysis. Brunauer–Emmett–Teller equation (BET) and quenched-solid density functional

theory (QSDFT) were used to get the specific surface area and the biocarbon pore-size distribution, respectively. Tapping density of biocarbon was estimated using graduated cylinder.

Fabrication and electrochemical characterization of supercapacitor

Symmetrical supercapacitors were fabricated as per our previous reports [22, 23] to evaluate the electrochemical performance of the synthesized biocarbon. Stainless steel (SS) plates with a surface area of 1.0 cm² were used as current collectors. The carbon slurry was prepared by blending wt.% 80 biocarbon and wt.% 10 carbon black in a mortar. PVDF (wt.% 10) was added into the mortar from the stock solution of PVDF/NMP. It was mixed well until it got the uniform carbon slurry by adding a required quantity of neat NMP. The carbon slurry was coated over one side of the well-polished SS plate and dried at 80 °C. Another side of the plate was masked by the non-conducting material to avoid interference with the electrochemical measurements, principally in the EIS. The active mass of the electrodes is in the range of ~ 10 mg/cm². The symmetrical supercapacitor was fabricated using two electrodes with almost equal mass loading. An aqueous solution of 1.0 M Na₂SO₄ and Whatman filter paper was used as an electrolyte and the separator in the symmetrical supercapacitor, respectively.

Electrochemical characterization of a symmetrical supercapacitor was carried out using a Biologic SP150 electrochemical workstation. EIS, CV and GCPL were used to evaluate the electrochemical performance of the symmetrical supercapacitors. EIS measurement was carried out in the frequency range from 100 kHz to 1 mHz with an amplitude of 10 mV at the open circuit potential. The self-discharge of the supercapacitor was evaluated by recording the open circuit cell potential (OCP) up to 100 h following the potential holding at identified stable cell voltage for 10 h [24]. The stability of the supercapacitors was measured by performing 10,000 GCPL cycles at 1.0 Ag⁻¹ for the selected cell potential. The stable cell potential was chosen strictly based on the coulombic efficiency of the supercapacitor. A digital Four-probe multimeter (model 34411A, Agilent) is used to measure DC electrical resistance at 100 kPa and 700 kPa [25].

The specific energy (E) of the symmetrical supercapacitor was evaluated from Eq. (1)[26, 27]:

$$E = \frac{I}{3.6m_{total}} \int_{t(U_{max})}^{t(U_{min})} U(t)dt \quad (1)$$

where the cell potential “ U ” (V) (U_{min} and U_{max} are the lower and higher cell potential limits respectively), total active mass “ m_{total} ” (g), time “ t ” (s) and current “ I ” (A).

The specific power (P) was evaluated from Eq. (2)[27, 28]:

$$P = \frac{E}{t_D} \quad (2)$$

where the discharge time “ t_D ” (s).

The capacitance of the cell (C_{cell}) was calculated from Eq. (3)[26, 27]:

$$C_{cell} = \frac{2E}{U_{max}^2} \quad (3)$$

The specific capacitance of a single electrode (C_{elec}) was calculated from Eq. (4)[26, 27]:

$$C_{elec} = \frac{2C_{cell}}{0.5m_{total}} \quad (4)$$

The coulombic efficiency (η_c) was calculated from Eq. (5) [26, 27]:

$$\eta_c = \frac{t_D}{t_C} \quad (5)$$

The variables t_D and t_C represent the time it takes to discharge (in seconds) and charge (in seconds), respectively.

The energy efficiency (η_E) was calculated from Eq. (6) [26, 27]:

$$\eta_E = \frac{E_D}{E_C} \quad (6)$$

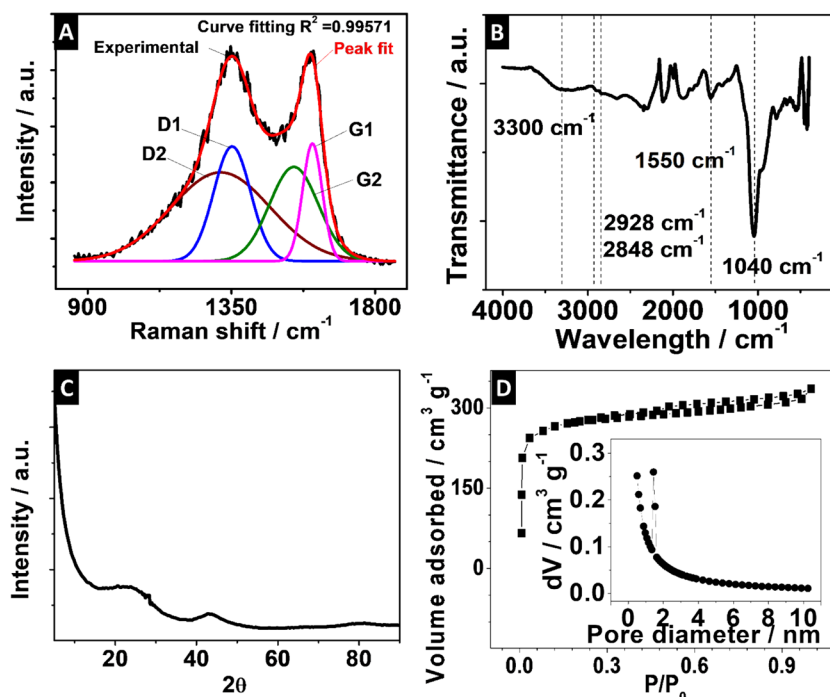
where E_D and E_C are the energy of the discharging and charging steps, respectively.

Results and discussion

Characterization of biocarbon

Laser Raman spectroscopy is a significant tool for characterizing carbon-based materials [29–31]. Figure 1A displays the laser Raman spectrum of biocarbon. It clearly shows two typical broad peaks at 1352 cm⁻¹ and 1603 cm⁻¹ corresponding to D and G bands, respectively. Out-of-plane vibrations resulting from structural defects of the honeycomb structure of the carbon network lead to a D-band. Typical G-band arises due to the in-plane vibrations of sp² carbon, a characteristic feature of carbon-base materials [2, 29]. The D and G-band are deconvoluted into 4 peaks by peak fitting viz. D1 (1352 cm⁻¹), D2 (1316 cm⁻¹), G1 (1603 cm⁻¹) and G2 (1546 cm⁻¹) bands [30, 31]. These 4 bands are classified into 2 pairs namely, G1 & D1 and G2 & D2, related to winding short basal planes with bond angle order and sp² cluster-like amorphous sp² carbon with bond disorder, respectively [30, 31]. The data obtained from the peak fitting, such as area fit, % area fit, FWHM, height and

Fig. 1 **A** Laser Raman spectrum, **B** FTIR spectrum, **C** XRD pattern and **D** nitrogen sorption isotherm (inset depicts the distribution of pores) of biocarbon



width, are given in Table S1 (ESI). The ratio of D/G bands is used to evaluate the degree of disorder in the graphite lattice [30, 31]. Instead of the intensity of peaks, it is better to use the area to calculate the A_D/A_G ratios. The A_{D1}/A_{G1} ratio is found to be 1.83. A high ratio indicates short basal plane size and high amorphous nature of the synthesized biocarbon [30, 31]. Similarly, A_{D2}/A_{G2} is also found to be 1.91. Also, a high A_{G2}/A_{G1} ratio of 1.99 indicates that high disordered content is a result of the reactive chemical activation process during the synthesis of biocarbon [31].

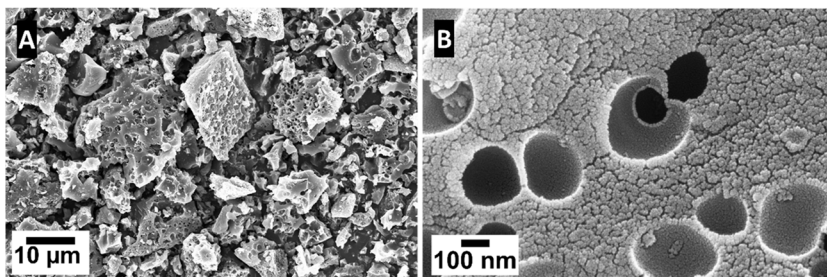
The surface functionalities of carbon materials were analysed by using the FTIR spectrum (Fig. 1B) [2]. It shows characteristic absorption bands of various functional groups. The stretching frequency of $-OH$ was noted at 3350 cm^{-1} . Symmetric and asymmetric stretching vibrational modes related to $-CH$ were observed as a pair of absorption bands at 2848 cm^{-1} and 2928 cm^{-1} [2, 32]. The absorption bands at 1040 cm^{-1} and 1550 cm^{-1} correspond to stretching vibrations of $-C-O$ and $-C=O$, respectively [2]. The presence of these functional groups was created during the chemical activation of biocarbon, which is in agreement with the laser Raman analysis.

XRD pattern of biocarbon with broad peaks is shown in Fig. 1C. Generally, the broad peaks are related to the amorphous nature of the biocarbon. The peaks at 26° and 43° were related to 002 and 100 of carbon material, respectively [2, 32]. In literature, the 002 peak position may be observed from 20° to 26° indicating the continuous increase of graphitization in the non-crystalline or amorphous carbon materials with an increase in temperature [32, 33]. An increase of the 2θ position of the 002 graphitic carbon plane

is associated with the reduction of the interplanar distance of graphic sheets. The position of the 002 planes in this work is in agreement with the previous literature [2, 32, 33]. Nitrogen sorption isotherm of biocarbon is shown in Fig. 1D, and insets show the pore-size distribution. GSA provides vital information about biocarbon, such as the surface area, pore volume and pore-size distribution. The sorption isotherm indicates that it belongs to the type-I pattern, as a long tail is seen at $<0.1 P/P_0$ [2, 34]. It is associated with the monolayer nitrogen sorption in the micropores indicating the synthesized biocarbon is nanoporous material. The estimated total surface area of $832\text{ m}^2\text{ g}^{-1}$ and the pore volume of $0.52\text{ cm}^3\text{ g}^{-1}$ were obtained by BET. The micropore volume ($<2\text{ nm}$) of $0.42\text{ cm}^3\text{ g}^{-1}$ confirms biocarbon is predominantly microporous in nature. Further, the pore-size distribution reaffirms the presence of micropores. The estimated average pore diameter is 2.4 nm . The tapping density of carbon was found to be 0.72 g/cm^3 .

FE-SEM images of biocarbon with two magnifications (3.5 KX and 200 KX) are shown in Fig. 2. SEM images of higher magnification (Fig. 2B) clearly show that the synthesized biocarbon is porous in nature. Probably, if we match the scale (100 nm) with porosity, the pores are in the range of micropores. Further, there are holes ($>100\text{ nm}$) seen in carbon particles which are formed by the vigorous interaction of carbon material with KOH during the chemical activation process. It may act as a local electrolyte reservoir which assists the diffusion of ions in the pores of the electrodes in the supercapacitors, and thus the electrochemical performance of the supercapacitor is vastly enhanced.

Fig. 2 FE-SEM of biocarbon at 2 different magnifications at **A** 3.5 KX and **B** 200 KX



Electrochemical characterization of supercapacitor

It is very important to investigate the electrochemical performance of the supercapacitors with high mass loading of the electrodes as it meets the requirements of commercial mass loading of $\geq 10 \text{ mg cm}^{-2}$ of active material[20]. Generally, thick electrodes (i.e. high mass load) inhibit the diffusion of ions into the electrode which affects the electrochemical performance. However, it is necessary to meet the critical requirement to get realistic and practical capacitance of the materials. Thus consciously, in the present work, symmetrical supercapacitors were fabricated with a mass loading of $\sim 10 \text{ mg cm}^{-2}$.

Electrical conductivity of biocarbon was estimated as 53.2 and 172.1 S m^{-1} at 100 and 700 kPa, respectively. EIS measurement was carried out to understand polarization resistance and diffusion of ions in the supercapacitor. Nyquist plot of the biocarbon-based symmetrical supercapacitor and its high-frequency region (inset) is shown in Fig. 3A. Typical high-frequency semicircle related to the charge transfer resistance (R_{ct}), diffusion process in the

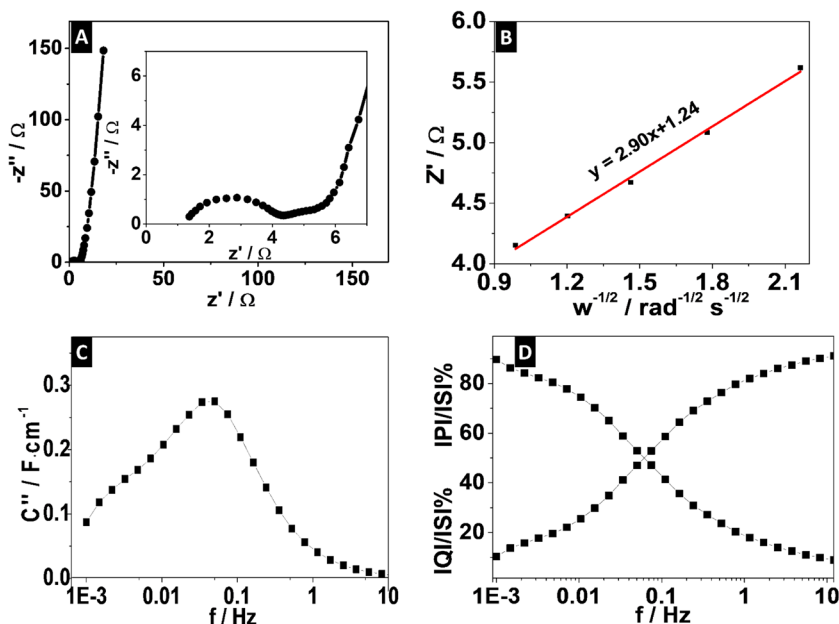
medium frequency and low-frequency vertical line are seen in the Nyquist plot [35–40]. The solution resistance (R_s) of 1.3Ω was measured with $1.0 \text{ M Na}_2\text{SO}_4(\text{aq.})$. R_{ct} is found to be $\sim 3.0 \Omega$ which depends on the nature and mass loading of the electrode, the type of the electrolyte, etc. Nevertheless, R_{ct} is compared with the reported aqueous supercapacitors with mass loading of electrode and electrolyte as follows: 0.35 to 0.46Ω (2.5 mg/cm^2 , 6 M KOH) [36], 0.25 to 1.0Ω (6 M KOH) [37], 6.99Ω (6 mg/cm^2 , $1 \text{ M H}_2\text{SO}_4$) [35] and 3.0Ω (10 mg/cm^2 , $1 \text{ M Na}_2\text{SO}_4$) (present work).

Further, the diffusion resistance (σ) was calculated from Eq. (7) to understand the charge–discharge kinetics, i.e. ion diffusion impedance of the fabricated device [36–38].

$$Z_w = \sigma \omega^{-1/2} - j\sigma \omega^{-1/2} \tag{7}$$

where Z_w is a Warburg impedance, $\sigma \omega^{-1/2}$ is a real part (Z') and $-j\sigma \omega^{-1/2}$ related to the imaginary part (Z''). The σ value can be calculated from the plot of z' and (frequency, ω) $^{-1/2}$ (Fig. 3B). The data from the selected Warburg region show a linear correlation, and the slope of the fitted line is σ which reflects the ion diffusion process.

Fig. 3 **A** Nyquist plot from electrochemical impedance spectroscopy (Inset: high-frequency region), **B** relationship between Z' and $\omega^{-1/2}$ in the low-frequency part calculated from EIS measurement results, **C** imaginary parts of complex capacitance vs. frequency and **D** plots of normalized active power, $|P|/|S|$ and reactive power $|Q|/|S|$ vs. frequency



The σ value is found to be 2.90 which is compared with 0.14 (Litchi derived biocarbon, 2.5 mg/cm², 6 M KOH) [36], 1.47 (zinc cobalt sulfide/AC, 2.5 mg/cm², 6 M KOH) [36] and 0.61 to 2.35 (2D porous carbon, 6 M KOH) [37]. It indicates that irrespective of the high-areal mass loading of 10 mg/cm², the fabricated device shows good charge–discharge kinetics. Further, low-frequency capacitive behaviour can be understood by inspecting the phase angle of the vertical line. The phase angle plotted against the frequency is shown in Fig. S1A. It is recognized that the ideal capacitor phase angle is 90°, while in the real condition, the phase angle closer to 90° indicates the excellent performance of the devices [35, 41]. The phase angle of the fabricated symmetrical supercapacitor is 84° indicating the good performance of the biocarbon supercapacitor in the present work.

Supercapacitors consist of a capacitor in the low-frequency region and a resistor in the high-frequency region. The transition from resistive to capacitive behaviour happens in the middle frequency [35, 42, 43]. The relaxation time constant (τ_o) or dielectric relaxation time constant is defined as the time taken to discharge 50% of the total energy stored in the supercapacitor. The real part of $c'(\omega)$ plotted vs frequency is shown in Fig. S1B. The capacitance and the frequency are inversely related to each other, and thus capacitance increases with decreasing the frequency. However, a plateau was observed after attaining maximum capacitance, indicating that capacitance is not entirely dependent on the frequency, at least in the low-frequency region. Similarly, the plot of the imaginary part of $C''(\omega)$ against frequency is shown in Fig. 3C. It shows that as the frequency decreases, the capacitance increases, and once it reaches its peak, the capacitance starts to decrease. The frequency (f_o) corresponding to the mid-point of the capacitance maximum of the real part of $C'(\omega)$ or the capacitance maxima of the imaginary part of $C''(\omega)$ is used to calculate the relaxation time constant (τ_o). Equation (8) can be used to calculate τ_o .

$$\tau_o = \frac{1}{2\pi f_o} \quad (8)$$

The τ_o of 2.52 s was calculated to the supercapacitor in the present work which is compared with 0.83 to 5.62 s for 4 types of 2D carbon nanosheet supercapacitors [37] and 2.6 s of symmetrical supercapacitor [35]. It demonstrates that irrespective of high mass loading the comparable τ_o value shows excellent diffusion of ions into the electrode. Similarly, normalized active and reactive power vs frequency is shown in Fig. 3D. These two factors are opposite to each other, and the crossover frequency (f_o) is also used to calculate the τ_o . The calculated τ_o value is in agreement with the value obtained from the real and imaginary parts of complex capacitance. Results obtained so far indicate

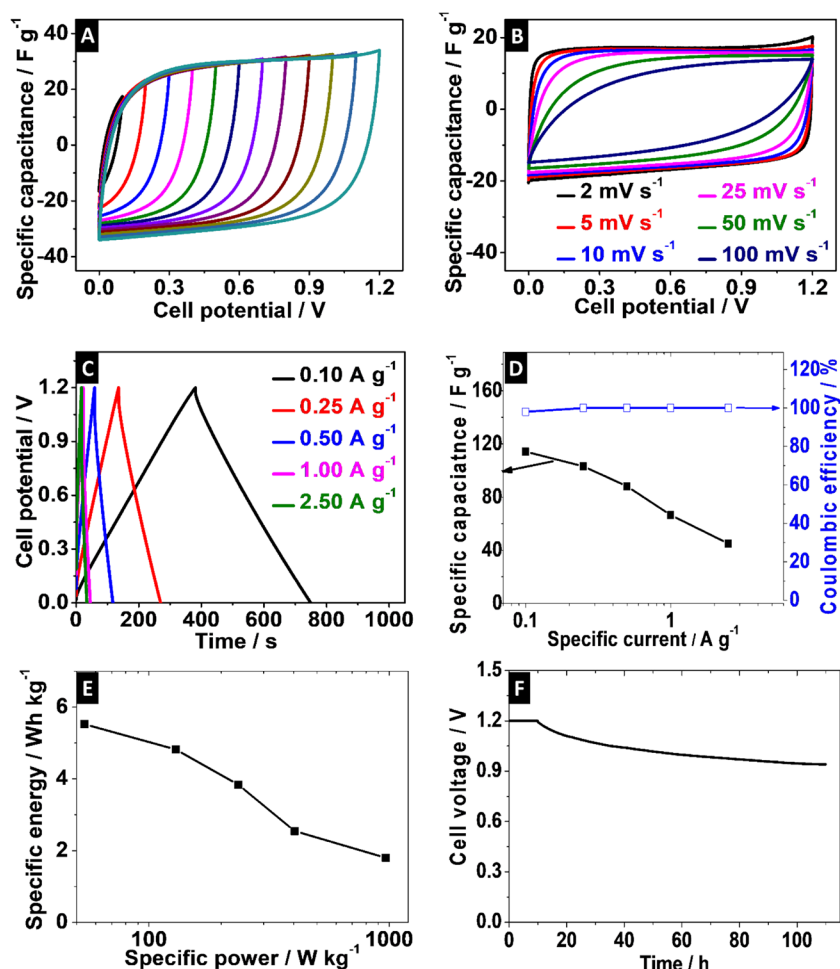
that supercapacitor with high mass loading have excellent charge–discharge kinetics which will be validated with CV and GCPL measurements.

Cell potential window opening of symmetrical supercapacitor was carried out by performing CV at 5.0 mV s⁻¹ in the potential interval of 100 mV s⁻¹ (Fig. 4A). Textbook rectangular CV profiles are recorded until the cell potential of 1.2 V, whereas a clear deviation from the rectangular profile as a result of gas evolution was noted beyond 1.2 V. Operating with the electrochemical decomposition of the electrolyte leads to the degradation of the electrode over the time; thus, maximum operable cell voltage is fixed as 1.2 V. Further, the scan rate effect for the cell potential of 1.2 V was carried out from 2.0 to 100 mV s⁻¹ which is shown in Fig. 4B. Irrespective of thick high mass loaded electrodes, the symmetrical supercapacitor exhibits good rate capability.

To validate the maximum cell potential of symmetrical supercapacitors, the GCPL was performed at the specific current of 0.1 A g⁻¹ at 1.2 V and 1.4 V. Coulombic efficiency is used to check the safely operable cell potential. At the cell potential of 1.2 V, the symmetrical supercapacitor that displays a healthy coulombic efficiency of ~99% was noted (Fig. 4C), while at 1.4 V, it is decreased to 90%, indicating the electrolyte degradation leads to the oxidative destruction of the carbon electrode in the long run. The rate capability for the identified maximum cell potential for the supercapacitor with the synthesized biocarbon was performed at different specific currents from 0.1 to 2.5 A g⁻¹ (Fig. 4C). The plot of specific capacitance and the coulombic efficiency vs the specific currents is shown in Fig. 4D.

The capacitance of 114 F g⁻¹ was estimated for an electrode in the symmetrical supercapacitor at a cell potential of 1.2 V at 0.1 A g⁻¹ with a coulombic efficiency of ~99%. The specific capacitance and active material mass loading of the supercapacitor in the present work were compared with the recently reported biocarbon supercapacitor (Table 1). It is clear that irrespective of the high mass loading, the fabricated supercapacitor displays good electrochemical performance. The capacitance decreases on increasing specific current; it is found to be 45 F g⁻¹ at 2.5 A g⁻¹. Besides the coulombic efficiency, the estimation of energy efficiency is an important step to understand the performance of the supercapacitors completely [26]. The variation of energy efficiency and the coulomb efficiency vs. specific currents are shown in Fig. S2 (ESI). The energy efficiency of 82% was noted for the supercapacitor at 0.1 A g⁻¹. The Ragone plot for the symmetrical supercapacitor is shown in Fig. 4E. The specific energy of 5.6 Wh kg⁻¹ and the specific power of 54 W kg⁻¹ were estimated at a cell voltage of 1.2 V at 0.1 A g⁻¹. The maximum power of 980 W kg⁻¹ was measured at 2.5 A g⁻¹. Self-discharge behaviour is an important parameter of the performance and efficiency of the supercapacitor. The self-discharge profile at 1.2 V of the

Fig. 4 **A** CV of cell potential window opening with the potential increment of 100 mV at 5.0 mV s⁻¹, **B** CV at different scan rates from 2 mV s⁻¹ to 100 mV s⁻¹, **C** GCPL profiles, **D** the specific capacitance and coulombic efficiency vs specific current, and **E** Ragone plot (the specific power vs specific energy) of biocarbon-based supercapacitor with 1.0 M Na₂SO_{4(aq)} at different specific current from 0.1 to 2.5 A g⁻¹ and **F** the self-discharge profile of the biocarbon based symmetrical supercapacitor at the call potential of 1.2 V



biocarbon-based supercapacitor is given in Fig. 4F. Recently, effective potential equalization and charge distribution of activated carbon electrodes were achieved with 3 h potential holding [24, 44]. Thus, in the present work, the initial potential holding at 1.2 V for 10 h was carried out to ensure no potential drop due to the charge redistribution of the supercapacitor. The OCP of the supercapacitor was monitored for the next 100 h to assess the self-discharge. Potential decay of 100 mV (8.3 mV h⁻¹) was noted after 12 h of OCP measurement. After 57 h, the cell potential reached 1.0 V, which is equivalent to a reduction of 3.5 mV s⁻¹. At the end of 100 h, the potential of 0.94 V was recorded with impressive no potential decay for the last 2 h of OCP measurement. Similar self-discharge profiles were reported in the literature for the commercial activated carbon-based supercapacitor [24, 44]. It indicates the biocarbon-based supercapacitor in the present work possesses low self-discharge behaviour.

Longevity of supercapacitors

Before reporting the electrochemical performance parameters, the measurement of the longevity of the symmetrical

supercapacitor is necessary. The long-term stability of the supercapacitor was evaluated at 1.0 A g⁻¹ up to 10,000 GCPL cycles. The capacitance retention vs the number of cycles is shown in Fig. 5. Initially, a significant increment of capacitance (~5%) was noted with 250 cycles, which may be due to the improved wettability of biocarbon electrodes on continuous charge–discharge cycling. Excellent capacitance retention of 100% was estimated at the end of 10,000 cycles, indicating the symmetrical supercapacitor capable of operating well beyond the tested number of cycles.

Conclusions

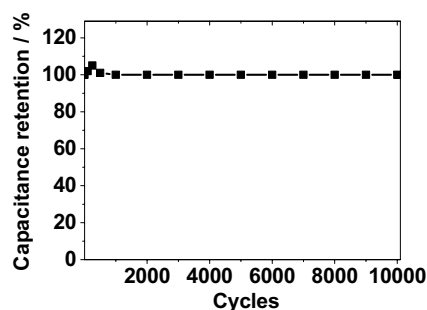
In this work, biocarbon was synthesized using *Datura stramonium* seeds and characterized using various characterization techniques. Research. Type I isotherm obtained by GSA reveals that the biocarbon is microporous in nature. The total surface area of 832 m² g⁻¹ and pore volume of 0.52 cm³ g⁻¹ (with 0.42 cm³ g⁻¹ of microporous volume) was estimated. The symmetrical supercapacitor with commercial-level mass loading of ~10 mg cm⁻² biocarbon showed a specific

Table 1 Comparison of mass loading and performance of biomass-based supercapacitors

S.no	Biomass	Electrolyte	Substrate	Mass loading	Specific capacitance	Number cycles	Capacitance retention
1	Corn stover	2 M KOH	Ni foam	-*	120 F g ⁻¹ at 0.05 A g ⁻¹	-*	-* [3]
2	Rice straw	1 M H ₂ SO ₄	SS foam	-*	156 F g ⁻¹ at 0.5 A g ⁻¹	10,000 at 3A g ⁻¹	88% [6]
3	Soybean pods	6 M KOH	Ni foam	-*	40F g ⁻¹ at 0.5 A g ⁻¹	10,000 at 5.0 A g ⁻¹	91% [9]
4	Egg yolk	6 M KOH	*	*	287 F g ⁻¹ at 0.5 A g ⁻¹	2000 at 2.0 A g ⁻¹	98% [16]
5	Potato waste residue	2 M KOH	Glassy carbon	0.08 mg**	225 F g ⁻¹ at 0.5 A g ⁻¹	5000 at 5.0 A g ⁻¹	94% [10]
6	Aloe vera	1 M H ₂ SO ₄	SS foam	~2 to 3 mg**	306 F g ⁻¹ at 0.5 A g ⁻¹	20,000 at 20 A g ⁻¹	83% [5]
7	Pistachio nutshell	6 M KOH	Ni foam	2.3 mg**	214 F g ⁻¹ at 0.5 A g ⁻¹	-**	** [14]
8	Casein	3 M KOH	Ni foam	4 mg **	95 F g ⁻¹ at 0.5 A g ⁻¹	-*	-*[4]
9	Walnut shell	PVA/KOH	-	4.0 mg **	225 F g ⁻¹ at 0.5 A g ⁻¹ (3- electrode setup)	3000 at 1 mA cm ⁻²	96% [13]
10	Wood waste	1 M H ₂ SO ₄	Platinum	2.0 mg cm ⁻²	295 F g ⁻¹ at 0.5 A g ⁻¹	10,000 at 10.0 A g ⁻¹	99.5% [11]
11	Lotus seedpods	6 M KOH	Ni foam	3.0 mg cm ⁻²	402 F g ⁻¹ at 0.5 A g ⁻¹	10,000 at 5.0 A g ⁻¹	95% [15]
12	Cinnamon sticks	NaClO ₄ in EC/DMC	SS steel	~2.5 to 3.5 mg cm ⁻²	271 F g ⁻¹ at 0.5 A g ⁻¹	300,000 at 4A g ⁻¹	80% [7]
13	Corn cob	6 M KOH	Ni foam	4–6 mg cm ⁻²	120 F g ⁻¹ at 1.0 A g ⁻¹	100,000 at 1.0A g ⁻¹	100% [8]
14	Rick husk	Deep eutectic solvent	Stainless steel	8 mg**	100 F g ⁻¹ at 0.1 A g ⁻¹	10,000 at 2.5A g ⁻¹	90% [2]
15	Daturastramonium seeds	1.0 M Na ₂ SO _{4(aq.)}	Stainless steel	~10 mg cm ⁻²	114 F g ⁻¹ at 0.1 A g ⁻¹	10,000 at 1.0 A g ⁻¹	100% This work

*Not reported

**Electrode area was not mentioned

**Fig. 5** Long-term stability of biocarbon-based supercapacitor with 1.0 M Na₂SO_{4(aq.)} at 1.2 V up to 10,000 cycles at 1.0 A g⁻¹

capacitance of 114 F g⁻¹ at the cell voltage of 1.2 V at 0.1 A g⁻¹. Excellent coulombic efficiency of 99% and energy efficiency of 82% were estimated at 0.1 A g⁻¹. The maximum

specific energy of 5.6 Wh kg⁻¹ at 0.1 A g⁻¹ and specific power of 980 W kg⁻¹ were measured at 2.5 A g⁻¹. Excellent specific capacitance retention of 100% was noted at the end of 10,000 GCPL cycles at 1.0 A g⁻¹ indicating that symmetrical supercapacitors with synthesized biocarbon possess high stability.

Supplementary Information The online version contains supplementary material available at <https://doi.org/10.1007/s11581-023-05181-x>.

Acknowledgements The authors thank PSG Management and Ultra Arts and Science College management for providing resources and their support.

Author contribution AK—conceptualization, methodology, experiments, providing resources, review and editing; SS—conceptualization, methodology, experiments, writing original manuscript, review and editing; Sadhana—carried out experiments and graph drawing.

Data availability All data used in this work are given in the manuscript.

Declarations

Ethical approval Not applicable.

Competing interests The authors declare no competing interests.

References

- Wang F, Harindintwali JD, Yuan Z et al (2021) Technologies and perspectives for achieving carbon neutrality. *Innovation* 2. <https://doi.org/10.1016/j.xinn.2021.100180>
- Sathyamoorthi S, Phattharasupakun N, Sawangphruk M (2018) Environmentally benign non-fluoro deep eutectic solvent and free-standing rice husk-derived bio-carbon based high-temperature supercapacitors. *Electrochim Acta* 286:148–157. <https://doi.org/10.1016/j.electacta.2018.08.027>
- Thakkar A, Shell KM, Bertolin M et al (2021) Production of levulinic acid and biocarbon electrode material from corn stover through an integrated biorefinery process. *Fuel Process Technol* 213:106644. <https://doi.org/10.1016/j.fuproc.2020.106644>
- Singh G, Bahadur R, Ruban AM et al (2021) Synthesis of functionalized nanoporous biocarbons with high surface area for CO₂ capture and supercapacitor applications. *Green Chem* 23:5571–5583. <https://doi.org/10.1039/d1gc01376a>
- Karnan M, Subramani K, Sudhan N et al (2016) Aloe vera derived activated high-surface-area carbon for flexible and high-energy supercapacitors. *ACS Appl Mater Interfaces* 8:35191–35202. <https://doi.org/10.1021/acsami.6b10704>
- Sudhan N, Subramani K, Karnan M et al (2017) Biomass-derived activated porous carbon from rice straw for a high-energy symmetric supercapacitor in aqueous and non-aqueous electrolytes. *Energy Fuels* 31:977–985. <https://doi.org/10.1021/acs.energyfuels.6b01829>
- Thangavel R, Kaliyappan K, Ramasamy HV et al (2017) Engineering the pores of biomass-derived carbon: insights for achieving ultrahigh stability at high power in high-energy supercapacitors. *Chemosuschem* 10:2805–2815. <https://doi.org/10.1002/cssc.201700492>
- Qu W-H, Xu Y-Y, Lu A-H et al (2015) Converting biowaste corn-cob residue into high value added porous carbon for supercapacitor electrodes. *Bioresour Technol* 189:285–291. <https://doi.org/10.1016/j.biortech.2015.04.005>
- Liu Z, Zhu Z, Dai J, Yan Y (2018) Waste biomass based-activated carbons derived from soybean pods as electrode materials for high-performance supercapacitors. *ChemistrySelect* 3:5726–5732. <https://doi.org/10.1002/slct.201800609>
- Ma G, Yang Q, Sun K et al (2015) Nitrogen-doped porous carbon derived from biomass waste for high-performance supercapacitor. *Bioresour Technol* 197:137–142. <https://doi.org/10.1016/j.biortech.2015.07.100>
- Ma X, Ding C, Li D et al (2018) A facile approach to prepare biomass-derived activated carbon hollow fibers from wood waste as high-performance supercapacitor electrodes. *Cellulose* 25:4743–4755. <https://doi.org/10.1007/s10570-018-1903-3>
- Yu J, Gao L, Li X et al (2016) Porous carbons produced by the pyrolysis of green onion leaves and their capacitive behavior. *New Carbon Mater* 31:475–484. [https://doi.org/10.1016/S1872-5805\(16\)60026-4](https://doi.org/10.1016/S1872-5805(16)60026-4)
- Xu X, Gao J, Tian Q et al (2017) Walnut shell derived porous carbon for a symmetric all-solid-state supercapacitor. *Appl Surf Sci* 411:170–176. <https://doi.org/10.1016/j.apsusc.2017.03.124>
- Xu J, Gao Q, Zhang Y et al (2014) Preparing two-dimensional microporous carbon from Pistachio nutshell with high areal capacitance as supercapacitor materials. *Sci Rep* 4:5545. <https://doi.org/10.1038/srep05545>
- Liu B, Zhou X, Chen H et al (2016) Promising porous carbons derived from lotus seedpods with outstanding supercapacitive performance. *Electrochim Acta* 208:55–63. <https://doi.org/10.1016/j.electacta.2016.05.020>
- Li J, Ma S, Cheng L, Wu Q (2015) Egg yolk-derived three-dimensional porous carbon for stable electrochemical supercapacitors. *Mater Lett* 139:429–432. <https://doi.org/10.1016/j.matlet.2014.10.133>
- Mutebi RR, Ario AR, Nabatanzi M et al (2022) Large outbreak of Jimsonweed (*Datura stramonium*) poisoning due to consumption of contaminated humanitarian relief food: Uganda, March–April 2019. *BMC Public Health* 22:623. <https://doi.org/10.1186/s12889-022-12854-1>
- Sharma M, Dhaliwal I, Rana K et al (2021) Phytochemistry, pharmacology, and toxicology of datura species—a review. *Antioxidants* 10:1291. <https://doi.org/10.3390/antiox10081291>
- Chadha A, Florentine S, Javaid M et al (2020) Influence of elements of climate change on the growth and fecundity of *Datura stramonium*. *Environ Sci Pollut Res* 27:35859–35869. <https://doi.org/10.1007/s11356-020-10251-y>
- Guo W, Yu C, Li S, Qiu J (2021) Toward commercial-level mass-loading electrodes for supercapacitors: opportunities, challenges and perspectives. *Energy Environ Sci* 14:576–601. <https://doi.org/10.1039/D0EE02649B>
- Jain A, Tripathi SK (2015) Almond shell-based activated nanoporous carbon electrode for EDLCs. *Ionics (Kiel)* 21:1391–1398. <https://doi.org/10.1007/s11581-014-1282-1>
- Sathyamoorthi S, Suryanarayanan V, Velayutham D (2015) Organo-redox shuttle promoted protic ionic liquid electrolyte for supercapacitor. *J Power Sources* 274:1135–1139. <https://doi.org/10.1016/j.jpowsour.2014.10.166>
- Sathyamoorthi S, Suryanarayanan V, Velayutham D (2014) Electrochemical exfoliation and in situ carboxylic functionalization of graphite in non-fluoro ionic liquid for supercapacitor application. *J Solid State Electrochem* 18:2789–2796. <https://doi.org/10.1007/s10008-014-2538-4>
- Sathyamoorthi S, Tubtimkuna S, Sawangphruk M (2020) Influence of structures and functional groups of carbon on working potentials of supercapacitors in neutral aqueous electrolyte: in situ differential electrochemical mass spectrometry. *J Energy Storage* 29. <https://doi.org/10.1016/j.est.2020.101379>
- Barroso-Bogeat A, Alexandre-Franco M, Fernández-González C et al (2014) Electrical conductivity of activated carbon–metal oxide nanocomposites under compression: a comparison study. *Phys Chem Chem Phys* 16:25161–25175. <https://doi.org/10.1039/C4CP03952A>
- Laheäär A, Przygocki P, Abbas Q, Béguin F (2015) Appropriate methods for evaluating the efficiency and capacitive behavior of different types of supercapacitors. *Electrochim Commun* 60:21–25. <https://doi.org/10.1016/j.elecom.2015.07.022>
- Sathyamoorthi S, Tejangkura W, Sawangphruk M (2020) Turning carbon-ZnMn₂O₄ powder in primary battery waste to be an effective active material for long cycling life supercapacitors: in situ gas analysis. *Waste Manag* 109:202–211. <https://doi.org/10.1016/j.wasman.2020.05.007>
- Lee J, Krüner B, Tolosa A et al (2016) Tin/vanadium redox electrolyte for battery-like energy storage capacity combined with supercapacitor-like power handling. *Energy Environ Sci* 9:3392–3398. <https://doi.org/10.1039/C6EE00712K>
- Ferrari AC (2007) Raman spectroscopy of graphite and graphite: disorder, electron–phonon coupling, doping and nonadiabatic effects. *Solid State Commun* 143:47–57. <https://doi.org/10.1016/j.ssc.2007.03.052>

30. Macedo JS, Otubo L, Ferreira OP et al (2008) Biomorphic activated porous carbons with complex microstructures from lignocellulosic residues. *Microporous Mesoporous Mater* 107:276–285. <https://doi.org/10.1016/j.micromeso.2007.03.020>
31. Hu S, Zhang S, Pan N, Hsieh Y-L (2014) High energy density supercapacitors from lignin derived submicron activated carbon fibers in aqueous electrolytes. *J Power Sources* 270:106–112. <https://doi.org/10.1016/j.jpowsour.2014.07.063>
32. Li Z, Reimer C, Picard M et al (2020) Characterization of chicken feather biocarbon for use in sustainable biocomposites. *Front Mater* 7:1–12. <https://doi.org/10.3389/fmats.2020.00003>
33. Arnold S, Rodriguez-Urbe A, Misra M, Mohanty AK (2018) Slow pyrolysis of bio-oil and studies on chemical and physical properties of the resulting new bio-carbon. *J Clean Prod* 172:2748–2758. <https://doi.org/10.1016/j.jclepro.2017.11.137>
34. Sathyamoorthi S, Sawangphruk M (2019) A simple and practical hybrid ionic liquid/aqueous dual electrolyte configuration for safe and ion-exchange membrane-free high cell potential supercapacitor. *Electrochim Acta* 305:443–451. <https://doi.org/10.1016/j.electacta.2019.03.090>
35. Sathyamoorthi S, Kanagaraj M, Kathiresan M et al (2016) Ethyl viologen dibromide as a novel dual redox shuttle for supercapacitors. *J Mater Chem A* 4:4562–4569. <https://doi.org/10.1039/c6ta00858e>
36. Dhakal G, Kumar DR, Sahoo S, Shim JJ (2023) Litchi seed biowaste-derived activated carbon supporting matrix for efficient symmetric and asymmetric supercapacitors. *Carbon N Y* 208:277–289. <https://doi.org/10.1016/j.carbon.2023.03.045>
37. Yu J, Yu C, Guo W et al (2019) Decoupling and correlating the ion transport by engineering 2D carbon nanosheets for enhanced charge storage. *Nano Energy* 64:103921. <https://doi.org/10.1016/j.nanoen.2019.103921>
38. Zhao Y, He J, Hu L et al (2023) Carboxyl-substituted organic molecule assembled with MXene nanosheets for boosting aqueous Na⁺ storage. *Small* 2304182:1–9. <https://doi.org/10.1002/sml.202304182>
39. Shi M, Wang R, Li L et al (2023) Redox-active polymer integrated with MXene for ultra-stable and fast aqueous proton storage. *Adv Funct Mater* 33. <https://doi.org/10.1002/adfm.202209777>
40. Wang R, Shi M, Li L et al (2023) In-situ investigation and application of cyano-substituted organic electrode for rechargeable aqueous Na-ion batteries. *Chem Eng J* 451:138652. <https://doi.org/10.1016/j.cej.2022.138652>
41. Shao Y, Li J, Li Y et al (2017) Flexible quasi-solid-state planar micro-supercapacitor based on cellular graphene films. *Mater Horizons* 4:1145–1150. <https://doi.org/10.1039/c7mh00441a>
42. Ganesh V, Pitchumani S, Lakshminarayanan V (2006) New symmetric and asymmetric supercapacitors based on high surface area porous nickel and activated carbon. *J Power Sources* 158:1523–1532. <https://doi.org/10.1016/j.jpowsour.2005.10.090>
43. Lust E, Jänes A, Arulepp M (2004) Influence of solvent nature on the electrochemical parameters of electrical double layer capacitors. *J Electroanal Chem* 562:33–42. <https://doi.org/10.1016/j.jelechem.2003.07.034>
44. García-Cruz L, Ratajczak P, Iniesta J et al (2016) Self-discharge of AC/AC electrochemical capacitors in salt aqueous electrolyte. *Electrochim Acta* 202:66–72. <https://doi.org/10.1016/j.electacta.2016.03.159>

Publisher's Note Springer Nature remains neutral with regard to jurisdictional claims in published maps and institutional affiliations.

Springer Nature or its licensor (e.g. a society or other partner) holds exclusive rights to this article under a publishing agreement with the author(s) or other rightsholder(s); author self-archiving of the accepted manuscript version of this article is solely governed by the terms of such publishing agreement and applicable law.